

# MICROFLUIDIC DETECTION OF SOIL NITRATE IONS USING NOVEL ELECTROCHEMICAL FOAM ELECTRODE

Md. Azahar Ali<sup>1</sup>, Kunal Mondal<sup>2</sup>, Yifei Wang<sup>1</sup>, Navreet K. Mahal<sup>3</sup>, Michael J. Castellano<sup>3</sup> and Liang Dong<sup>1</sup>

<sup>1</sup>Department of Electrical and Computer Engineering, Iowa State University, Ames, Iowa 50011, USA

<sup>2</sup>Department of Chemical and Biomolecular Engineering, North Carolina State University, Raleigh, North Carolina 27695, USA

<sup>3</sup>Department of Agronomy, Iowa State University, Ames, Iowa 50011, USA

## ABSTRACT

This paper reports on a novel sensing interface using composites of graphene foam-titanium nitride nanofibers integrated into a microfluidic sensor for measurement of soil nitrate ions. An *in-situ* microfabrication approach, based on liquid phase polymerization process, is developed to enable integration of the porous composite into microfluidic channels. This sensor provides an ultralow limit-of-detection of 0.01 mg/L, and a high sensitivity of 683.3  $\mu\text{A mg}^{-1}\text{L cm}^{-2}$  for nitrate ions. The advantageous features of composite, in conjunction with the *in-situ* integration approach, will enable a promising microfluidic sensor platform to monitor soil ions for nutrient management towards sustainable agriculture.

## INTRODUCTION

Microfluidic sensors provide many benefits such as high portability, low consumption of agents and reagents, high sensitivity, fast response, and process parallelization.<sup>1</sup> Integration of nanostructured functional materials into microfluidic sensors has demonstrated a potential to enhance biological and chemical sensing capabilities.<sup>2</sup> Carbon nanotubes and zinc oxide nanowires were integrated into microfluidic electrochemical sensors for the detection of chemical species with improved sensitivity and stability, owing to an increased sensing surface area and electrochemical reactivity.<sup>2,3</sup>

Graphene foam (GF) has recently demonstrated to provide a powerful platform to biochemical sensing and the networked interior surfaces of GF provide a suitable environment to attract functional nanomaterials via electrostatic interactions.<sup>4</sup> Consequently, several GF-based composites have been developed as electrochemical electrode materials via surface functionalization with various metal oxides.<sup>5</sup> It is believed that the composites of GF and nanomaterials are strong candidates for new-generation microfluidics-based electrochemical sensors, owing to their fast transport of charge carriers, large surface area, high electrical conductivity and mechanical strength, and ease of functionalization with receptor biomolecules. However, GF and GF-based composites appear porous with irregular pore shapes and rough external surfaces that are unfavorable for photolithography; in addition, they are relatively thick at millimeter (mm) or sub-mm scale with networked scaffold structures<sup>6</sup> that are unfavorable for directional deep etching. Therefore, direct patterning of GF and GF-based composites or creating of microfluidic structures inside the materials is challenging to achieve by conventional photolithography and etching techniques. This has significantly limited their applications in microfluidic sensors and other devices. The manual

assembly process was relatively complex and had limited control over the position of the patterns. In addition, the assembled structure had relatively low robustness.

Functionalized nanofibers (NFs) can provide many excellent properties suitable for chemical and biological sensor applications, including high aspect ratio, large surface area, and high electrochemical reactivity.<sup>7</sup> In particular, when NFs-based titanium dioxide ( $\text{TiO}_2$ ) functionalized with biomolecules, electrochemical conductivity of  $\text{TiO}_2$  NFs significantly reduces, owing to the presence of oxygen vacancies and Ti-O bonds that restricts electron transfer.<sup>8</sup> To overcome this issue, researchers have recently developed nanostructured titanium nitride (TiN) by replacing oxygen at  $\text{TiO}_2$  with nitrogen to achieve improved electrical conductivity, electron transport rate, and chemical stability.<sup>9,10</sup> However, TiN NFs have *little* been explored in the area of electrochemical based biochemical sensors.

Here we report on an *in-situ* integration method to seamlessly assemble a novel nanocomposite of GF-TiN NFs and a microfluidic channel together to realize a high-performance electrochemical soil nutrient sensor. Liquid-phase polymerization process (LP<sup>3</sup>)<sup>16</sup> is employed to overcome the difficulty of assembling any GF or GF-based composites into microfluidic devices associated with the porous and irregular-shaped interior structure, poor surface morphology, and large thickness of these porous materials. We demonstrate *in-situ* formation of microfluidic channels within or across the GF-TiN scaffolds. This makes it convenient to realize a microfluidic sensor using the GF-TiN NFs as an electrochemical electrode material. While the GF-TiN NFs composite can be tailored to detect a variety of biochemical molecules through appropriate surface functionalization, we present a microfluidic nitrate sensor by immobilizing nitrate reductase (NaR) enzyme onto the embedded GF-TiN NFs composite to form NaR/GF-TiN NFs based bio-scaffolds. This is owing to an emerging global interest in sustainable agriculture and environment, where nitrogen (N) is one of the most important macronutrients for crop production in agriculture.<sup>11-15</sup> The precise and timely measurement of the availability of plant nutrients in soil can enable a precise nutrient application in farming.<sup>11-15</sup> By monitoring soil nitrate dynamics, farmers can optimize the N fertilizer inputs to enhance crop productions. Managing nitrate input to agricultural soils can result in substantial economic return for farmers.

## DEVICE FABRICATION

To synthesis TiN NFs,  $\text{TiO}_2$  NF were first synthesized by electrospinning technique using a  $\text{Ti(OiPr)}_4$  precursor

material.<sup>8</sup> After that, the TiO<sub>2</sub> NFs was subjected to heat treatment in presence of inert argon gas and ammonia atmosphere at 950 °C for 2 hr. The carbonization occurred to the residual carbon from the unburned PVP polymer, and ammonia gas started the conversion of TiO<sub>2</sub> to titanium oxynitride (TiO<sub>x</sub>N<sub>y</sub>) phase by doping of N into TiO<sub>2</sub> system. Subsequently, the argon flow was removed and only NH<sub>3</sub> exposed to 1050 °C, at which the TiO<sub>2</sub> NFs were completely converted into TiN NFs.<sup>9,10</sup> Also a small amount of carbon content was present at TiN NFs which could help bind with NaR enzyme molecules via covalent interactions.

The sensor consists of a working electrode placed between Au and Ag/AgCl electrodes (Fig. 1) in a channel. Au (counter) and Ag/AgCl (reference) electrodes are patterned on a SiO<sub>2</sub> layer grown on a Si wafer. The dispersion solution (50 μL) of TiN NFs (2 mg/mL) in ethanol was drop coated at a pre-cut GF and then rested for 2 hr to form a composite of GF-TiN NFs (4 mm × 2.4 mm × 1.1 mm). Then, the composite was treated with oxygen plasma to produce functional groups (-COOH) and then positioned between the Ag/AgCl and Au electrodes. The LP<sup>3</sup> process was used to integrate the GF-TiN NFs composite and other electrodes into a microfluidic channel. Following that, 1.1-mm-thick PDMS spacers (with the same thickness of the GF-TiN NFs composite) were emplaced between the device substrate and a 1-mm-thick top glass slide to form an air cavity. The top glass slide was pre-punched to form two through-holes as an inlet and an outlet of a channel using a conventional milling machine with a 1-mm-diameter diamond drill bit. Separately, a photopatternable precursor solution was prepared by mixing monomer—isobornyl acrylate (IBA), crosslinker—tetraethylene glycol dimethacrylate (TeGDMA), and photoinitiator—2, 2-dimethoxy-2-phenylacetophenone (DMPA) at a weight ratio of 31.66:1.66:1.0.<sup>16</sup> The precursor solution was injected into the cavity using a conventional plastic pipette. After that, a transparency film based photomask was placed on top of the glass slide and exposed under an ultraviolet light (12 mW cm<sup>-2</sup>) for 95 s. The channel was formed due to polymerization and rinsed the device in ethanol to remove unpolymerized precursor. The device was baked on a hotplate at 60 °C for 1 hr to remove solvents. Therefore, the in-situ assembly of the GF-TiN NFs into the microfluidic channel was realized (Fig. 2). Finally, the embedded GF-TiN NFs composite was functionalized with NaR enzyme molecules using EDC-NHS coupling chemistry. The SEM image (Fig. 1c) of a GF-TiN composite and TEM images (Fig. 1d-e) for electrospun TiN NFs showing hexagonal crystals connected along the fiber axis.

Because the photosensitive precursor solution has a low viscosity and high transparency, it can easily fill in the irregular-shaped interior structures of porous materials during the LP<sup>3</sup> process. Due to the fluid nature, the unpolymerized precursor solution will be easily removed by flushing the channel with water or ethanol, provided that the channel is high enough not to be blocked by individual scaffolding materials (note: 100 – 150 μm-thick nickel was used as the base scaffolding

material of GF). The spatial resolution of channels may be improved by fine-tuning photopolymerization conditions, and optimizing the shapes and dimensions of scaffolding materials for minimizing the light scattering and reflection effects. This integration method does not utilize any spinning or casting of photosensitive materials, wherein, self-planarization of the rough external surfaces of GF can be achieved. The whole process of integrating channels and the GF and GF-based composites requires only about a couple of minutes, eliminating complex and inaccurate manual assembly steps.

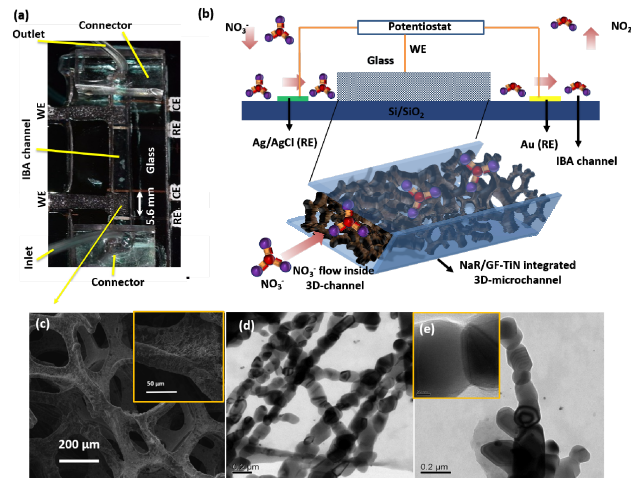


*Figure 1: A photograph of the fabricated sensors for nitrate detection where two sensors are formed in a channel. (b) Schematic representation of the device. Inset shows a 3D view of NaR/GF-TiN electrode integrated with a channel. (c) SEM image of part of a GF-TiN electrode and (d-e) TEM images for electrospun TiN NFs showing hexagonal crystals connected along the fiber axis. TiN NFs were produced by replacing O<sub>2</sub> in TiO<sub>2</sub> NFs under argon and ammonia gas treatment at ~1050 °C.*

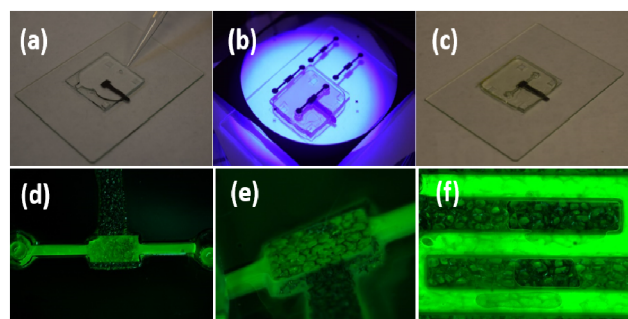


*Figure 2: (a-d) Photographs of the LP<sup>3</sup> process for integration of GF-TiN electrode within a channel. (d, e) Fluorescence images showing the integration of GF-TiN electrode into a channel. The composite electrode is ~1.1-mm-thick. (f) Fluorescence image showing the formation of a serpentine microfluidic channel inside a GF material using the same process shown in (a-d).*

## RESULTS AND DISCUSSION

Chronoamperometry is a widely used amperometric method to monitor transient response of the working electrode of electrochemical sensor with a potential pulse (versus the reference electrode). This method has a fast response and a high signal-to-noise ratio, compared to other amperometric techniques.<sup>17</sup> We conducted chronoamperometric measurements for the sensor with synthetic test samples of nitrate concentrations ranging from 0.01 to 442 mg/L mixed in a PBS solution. Analyte solutions are injected through the inlet of the channel. Although the NaR/GF-TiN NFs composite is embedded in the channel, the analytes can easily pass through the interior pores of the composite and exit at the outlet of the channel. The sensing potential is maintained at -0.2 V during the measurement, at which the immobilized *NaR* enzyme molecules dominate the specific reductive reaction at the electrode. Figure 3a shows that the transient responses of the sensor exposed to different nitrate concentrations. The calibration curve of the sensor shown in Fig. 3b demonstrates that the chronoamperometric current increases almost proportional to logarithm of nitrate concentration over the whole range of concentration tested. The sensitivity of the sensor is calculated to be  $683.3 \mu\text{A mg}^{-1}\text{L cm}^{-2}$  based on the calibration curve. Using the NaR/GF-TiN NFs bioelectrode, the sensor is capable to detect a minute concentration of nitrate ions at 0.01 mg/L.

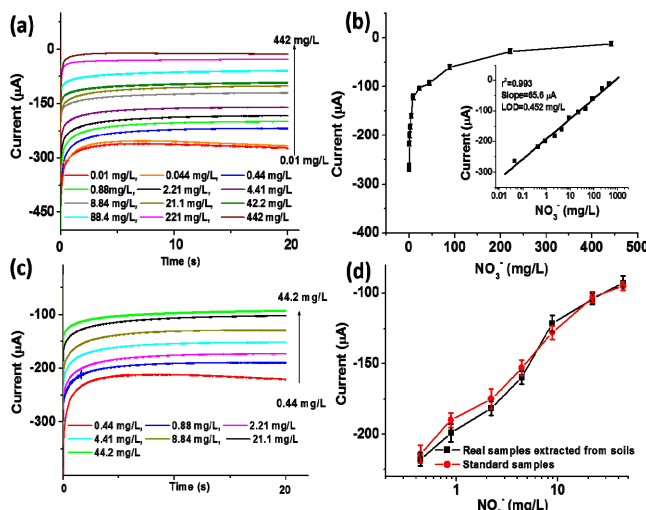


Figure 3: (a) Chronoamperometric responses of the sensor as a function of nitrate concentration from 0.01 to 442 mg/L, (b) Sensor calibration plot showing current vs nitrate concentration. Inset shows the plot of logarithms of the nitrate concentration with output current. (c) Chronoamperometric responses of the sensor to nitrate concentrations in real sample extracted from soils. (D) Comparisons of current vs. nitrate concentration for detecting nitrate ions in synthetic and real soil samples.

Next, we validate the sensor with NaR/GF-TiN NFs bioelectrode to detect nitrate concentrations of real solution samples extracted from the soil collected from a *Ze a mays* farm field. In this measurement, -0.2 V is used

as a sensing potential and the soil solutions are mixed with a PBS solution (pH = 7.4) containing [Fe(CN)<sub>6</sub>]<sup>3-/4-</sup> and injected into the embedded channel. Figure 3c presents the chronoamperometric currents of the sensor responding to different nitrate concentrations of soil solutions. As the concentration increases, the chronoamperometric current is found to increase due to the catalytic reduction of nitrate ions in the presence of NaR on the sensor surface (Fig. 3d). The average relative standard deviation (RSD) for the output current is less than  $\pm 4\%$  for the real samples with the nitrate concentrations of 2.21, 4.41, 8.84 and 22.1 mg/L, however, the value of RSD decreases to even only  $\pm 1\%$  for 0.44, 0.88 and 44.2 mg/L concentrations (Fig. 3d). Therefore, this sensor demonstrates the considerable ability to quantify nitrate concentrations in the soil solution samples.

For the detection of nutrient ions in soil solutions, common measurement practices include using ion chromatography,<sup>18</sup> spectrophotometry,<sup>19</sup> ion-selective electrodes (ISEs),<sup>20</sup> and electrochemical sensors.<sup>14-18</sup> Among these, chromatography and spectrophotometry are limited to laboratories. The ISE-based and electrochemical sensors are field deployable and can convert the activity of a specific ion in a solution into an electrical signal. **Table 1** compares the performances of our sensor with other reported electrochemical nitrate sensors. Our sensor provides a wide dynamic range of nitrate concentration from 0.01 to 442 mg/L. The use of NaR/GF-TiN NFs bioelectrode results in a significantly increased sensitivity ( $683.3 \mu\text{A mg}^{-1}\text{L cm}^{-2}$ ) and decreased LOD for the detection of nitrate compared to the sensors using other nanostructured materials, such as reduced graphene oxide,<sup>14</sup> carbon nanotubes-polypyrrole,<sup>15</sup> wrinkled graphene oxide,<sup>16</sup> poly(3,4-ethylenedioxythiophene)-GO,<sup>21</sup> and Ag@iron oxide.<sup>17</sup> The improved performances of our sensor may be owing to an enhanced electrochemical reactivity of the NaR/GF-TiN NFs bioelectrode as it enables an improved loading capacity of enzyme molecules for catalytic reactions.

**Table 1. Sensor performance compared with other reported electrochemical sensors**

Materials	Nitrate Con. Range	Sensitivity	Ref.
rGO	8.9-167 μM	$27 \text{nA}/\mu\text{M}/\text{cm}^2$	14
CNT-Polypyrrole	440-1450 μM	$0.3 \text{nA}/\mu\text{M}/\text{cm}^2$	15
Wrinkled GO	1-100 μM	$0.224 \mu\text{A}/\mu\text{M}/\text{cm}^2$	16
Silver@iron oxide	0-1000 μM	$0.663 \mu\text{A}/\mu\text{M}/\text{cm}^2$	17
Polypyrrole	50 – 5000 μM	NA	18
GF-TiN	0.01-442 mg/L or 0.16-7128 μM	$683.3 \mu\text{A mg}^{-1}\text{L cm}^{-2}$ or $42.1 \mu\text{A}/\mu\text{M}/\text{cm}^2$	This work

Effects of interfering ions for the GF-TiN NFs based sensor are also investigated (Fig. 4a, b). A few types of interfering ions are included in the selectivity test, including sulfate (SO<sub>4</sub><sup>2-</sup>; 50 μM concentration), potassium (K<sup>+</sup>; 200 μM), chloride (Cl<sup>-</sup>; 450 μM), and bicarbonate (HCO<sub>3</sub><sup>-</sup>; 100 μM). These ions are chosen because they are important anions and cations in

agricultural soils. The concentration of nitrate ion is kept same at 442 mg/L for all the cases. The measurements are conducted at a potential of -0.2 V (Fig. 4a). As shown in the chronoamperometric responses of the sensor to these interfering ions (Fig. 4b), this sensor shows a good selectivity in the presence of the aforementioned interfering ions, as demonstrated by their RSD of  $\pm 2.4\%$  from the initial values of current. Because the immobilized NaR enzyme molecules on the surface of GF-TiN composite restrict themselves from reducing oxo-compounds such as chloride, sulfate, and nitrite, the influences of different interfering ions are largely minimized for measuring complex real soil samples.

Furthermore, the stability of the sensor is evaluated at a 5-day interval over 30 days. The stability test involves exposing the sensor to the real soil solution sample (nitrate concentration: 8.84 mg/L), and when not in use, storing the sensor in 4 °C. The result in Fig. 4c indicates that the sensor performance is considerably stable with a RSD value of  $\pm 2\%$  from its initial response. In addition, for reproducibility test (Fig. 4d), four identical sensors are prepared and chronoamperometric measurements are conducted with the same concentration of nitrate (44.2 mg/L). A RSD of  $\pm 5.3\%$  from the initial current signal demonstrates a good reproducibility of the sensor for the detection of nitrate ions.

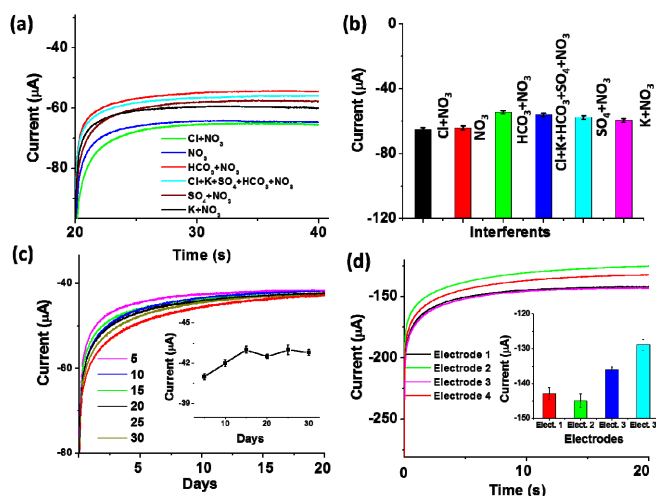


Figure 4: (a) Current responses of the microfluidic sensor to interfering ions ( $\text{Cl}^-$ ,  $\text{K}^+$ ,  $\text{HCO}_3^-$ , and  $\text{SO}_4^{2-}$ ) at a potential of -0.2 V. (b) The current responses for selectivity test versus different concentrations of nitrate ions. (c) Stability test for fabricated device, inset showing current versus number days and (d) reproducibility test for different fabricated sensors, inset showing the current with respect to different sensors.

## CONCLUSIONS

In summary, we have demonstrated the in-situ integration of porous GF-TiN NFs composites and microfluidic channels to realize high-performance microfluidic electrochemical sensors. The in-situ assembly process utilizes the simple LP<sup>3</sup> process, which enables convenient

embedding of the GF-based electrochemical electrode into microfluidic channels. As a result, the embedded GF-TiN NFs based scaffolds allow analyte solutions to flow through and interact with the biomolecules covalently immobilized on the surface of scaffolds. In addition, the unique combination of TiN NFs and GF produces synergy that benefits generating a high-performance electrochemical electrode that provides the improved electrochemical reactivity, heterogeneous electron transfer rate, and loading capacity of receptor biomolecules specific to target analytes.

The sensor provides a high sensitivity, a low LOD, and good reproducibility. This present sensor technology will be adopted to the detection of different ionic nutrients in soils such as phosphate, chloride and potassium ions, as well as other target biomolecules in many other applications, by functionalizing the GF-TiN NFs-based electrodes with different specific molecules. It is believed that the present approach will lay a firm foundation to facilitate exploration of various GF-based microfluidic sensors for many emerging applications.

## ACKNOWLEDGEMENTS

This work is supported in part by the Iowa State University's Plant Sciences Institute, the Iowa Corn Promotion Board, and the U.S. National Science Foundation under grants DBI-1353819, CCF-1331390, IIP-1602089, and IOS-1650182.

## CONTACT

\*L. Dong, tel: +1- 515-294-0388; ldong@iastate.edu

## REFERENCES

- [1] E. K. Sackmann et al., *Nature*, 2014, 507, 181-9.
- [2] J. Kim, Z. Li et al., *Lab Chip*, 2011, 11, 1946-51.
- [3] D. Vilela, et al., *Anal. Chem.*, 2012, 84, 10838-44.
- [4] Z. Chen, W. Ren, et al., *Nat. Mater.*, 2011, 10, 424-8.
- [5] X. C. Dong, H. Xu, et al., *ACS Nano*, 2012, 6, 3206-13.
- [6] Z. Chen, W. Ren, et al., *Nat. Mater.*, 2011, 10, 424-8.
- [7] D. Li and Y. Xia, *Nano Lett.*, 2003, 3, 555-60.
- [8] K. Mondal, et al., *ACS Appl. Mater. Interfaces*, 2014, 6, 2516-27.
- [9] J. H. Bang, et al., *Adv. Mater.*, 2009, 21, 3186-3190.
- [10] H. Li, et al., *Adv. Funct. Mater.*, 2013, 23, 209-14.
- [11] V. Mani, et al., *Electrochim. Commun.*, 2012, 17, 75-78.
- [12] F. Can, et al., *Mater. Sci. Eng. C*, 2012, 32, 18-23.
- [13] Md. A. Ali, et al., *RSC Adv.*, 2016, 6, 67184.
- [14] M. Bonyani, et al., *Electroanalysis*, 2015, 27, 2654.
- [15] M. Sohail, et al., *Electroanalysis*, 2009, 21, 1411.
- [16] D. J. Beebe, et al., *Proc. Natl. Acad. Sci.*, 2000, 97, 13488-93.
- [17] Md. A. Ali, et al., *Sci. Rep.*, 2013, 3(2661), 1-9.
- [18] K. Ito, et al., *J. Chromatogr. A*, 2005, 1083, 63-7.
- [19] K. M. Miranda, et al., *Nitric Oxide*, 2001, 5, 62-71.
- [20] J. E. Davies, et al., *Analyst*, 1972, 97, 87-94.
- [21] Md. A. Ali, et al., *Sens. Actuator B-Chem.*, 2017, 239, 1289-1299.